HHS Public Access

Author manuscript

Mol Carcinog. Author manuscript; available in PMC 2019 November 01.

Published in final edited form as:

Mol Carcinog. 2018 November ; 57(11): 1640–1650. doi:10.1002/mc.22886.

The *Rb* tumor suppressor regulates epithelial cell migration and polarity

Tiziana Parisi[1], **Michele Balsamo**[1], **Frank Gertler**[1,2], and **Jacqueline A. Lees**[1,2]

[1]The David H. Koch Institute for Integrative Cancer Research Cambridge, MA 02139, USA.

[2]Department of Biology, Massachusetts Institute of Technology, Cambridge, MA 02139, USA.

Abstract

Altered cell polarity and migration are hallmarks of cancer and metastases. Here we show that inactivation of the retinoblastoma gene (*Rb*) tumor suppressor causes defects in tissue closure that reflect the inability of *Rb* null epithelial cells to efficiently migrate and polarize. These defects occur independently of pRB's anti-proliferative role and instead correlate with upregulation of RhoA signaling and mislocalization of apical-basal polarity proteins. Notably, concomitant inactivation of *tp53* specifically overrides the motility defect, and not the aberrant polarity, thereby uncovering previously unappreciated mechanisms by which *Rb* and *tp53* mutations cooperate to promote cancer development and metastases.

Introduction

Motility and polarity are interconnected processes that play key roles in development, wound healing, and cancer. These processes are regulated by the family of small Rho GTPases and the PAR complex respectively, with extensive cross-talk between them. In the active GTP-bound state, the GTPases trigger signaling cascades that shape the actin cytoskeleton by regulating cell protrusions, focal adhesions and stress fibers, thereby establishing front-back polarity and allowing cell migration [1,2]. The PAR proteins regulate apical-basal polarity during tissue morphogenesis by creating functional and spatial distinct domains within a cell via correct assembly and positioning of adherens and tight junctions [3,4]. The PARs cooperate with Rho GTPases to establish tissue polarity, and also with the planar cell polarity machinery, which acts to align epithelial appendices along the body front-rear axis [5–7]. Additionally, the PARs regulate symmetric and asymmetric cell division, thereby influencing stem cell differentiation and regeneration [8]. Given these functions, it is unsurprising that RhoGTPases and PARs are frequently deregulated in cancer. Notably, direct mutation of these genes rarely occurs and instead these factors are typically deregulated through altered expression, localization and/or activity [5]. This finding led to speculation that these factors are regulated by cancer genes in tumors and potentially normal physiology. Accordingly, numerous oncogenes (e.g. kras, c-jun, and EGFR), as well as a few tumor suppressors (NF2, Apc and LKB1), have been shown to modulate signaling pathways

Author contributions: Conceptualization and planning, T.P. and J.A.L.; Methodology and Investigation, T.P. and M.B.; Data interpretation, T.P., M.B., F.G. and J.A.L.; Writing: T.P. and J.A.L.; Supervision: F.G. and J.A.L; Funding Acquisition: J.A.L.

that impact migration and polarity. Moreover, it was recently shown that cell motility pathways must be deregulated for effective primary tumor development, as well as for the invasive phase [9]. This suggested that engagement of the cell mobility machinery may be a more general effect of early cancer mutations.

The human *RB-1* gene is mutated in about a third of human tumors, typically at an early stage. Its protein product, pRB, is best known for restraining proliferation by repressing E2F transcription factors [10]. However, pRB has been shown to regulate other biological processes including fate commitment, chromosomal integrity, apoptosis and metabolism, primarily through interaction with transcription factors but also via transcriptionally-independent, and even non-nuclear, mechanisms [10]. Notably, a potential role for pRB in migration and polarity remains under-investigated, likely because phenotypes characteristic of migration and polarity defects can easily be misinterpreted as arising from ectopic proliferation. Still, *Rb* loss has been shown to decrease tangential migration of neurons, augment invasiveness in prostate cancer cells, and cause planar cell polarity defects in Drosophila [11–13]. Here we show that *Rb* deficiency yields developmental and wounding defects in mouse models, which are cell autonomous and independent of ectopic cell proliferation, and instead reflect a profound impairment in both the motility and polarity of *Rb* mutant epithelial cells.

Materials and Methods

Mice, keratinocytes, IHC and IF:

Mice used in this study were: *Rb* and *Rb;E2f* chimeras [14,15]; $Rb^{c/c}$ [16]; *K14Cre* [17]; and K14CreERT [18]. Tissues were treated and stained as described previously [14], or OCT-embedded for histology and IHC. Primary keratinocytes were isolated from E18.5 embryos and cultured as described previously [19] in 0.05 mM $CaCl_2$ on Col1 coated surfaces. AdGFP and AdCreGFP infections were conducted at 10 MOI for 3 hrs. Junctions were induced with 1.8mM Ca2+. Rock inhibitors (Calbiochem) were added at 10μM Y27632 and 5 μM H-1152, and BrdU at 33μM. For IF, 10 μm cryosections or coverslips fixed with 4% PFA for 15’ were incubated o/n at 4°C with primary antibodies and detected with Alexa Fluor-conjugated secondary antibodies (Invitrogen), plus Alexa Fluor-conjugated phalloidin and dapi, to also visualize F-actin and nuclei. DeltaVision microscope images were deconvolved using SoftWoRx acquisition software (Applied Precision) and quantified by ImageJ. P values were calculated with Student’s t-test.

Migration and wound healing assays:

For Boyden chambers, 10^5 cells were plated in triplicate on 8μm pore, 24 well transwell plates. Migrated cells were detected by crystal violet after removing cells from the top chamber by Q-tip. For *in vitro* scratch assays, confluent cell layers were incubated with 1.8mM Ca for >24 hrs and scratched with yellow tips. Two wounded areas/plate/embryo were photographed over time and the gaps quantified by ImageJ. For time lapse microscopy, 5×10^4 cells were plated on 12 well glass bottom plates (MatTek), photographed every 10 min for 15 hours and the GFP+ cells analyzed by Imaris imaging software. P values were calculated with Student’s t-test. For *in vivo* wound healing, 2 months littermates were

painted with tamoxifen (2.5 mg in EtOH) for 11 days, and a skin-thick 1 cm incision monitored daily for 5 days. Genomic DNA was extracted and analyzed by PCR.

Protein and RNA:

For protein, cells were lysed in NP40 buffer+ protease and phosphatases inhibitors, or 1% SDS 60mM Tris-Cl pH 6.8 at 95°C, and processed as described [14]. For mRNA, total RNA was extracted using RNeasy Mini+RNAse-Free DNAse Set kits (Quiagen). cDNA was generated using Superscript III (Invitrogen) and 10ng/sample (≥3 cell lines) assayed in duplicate by qPCR on a 7500 real time PCR system (Applied Biosystem) using SybrGreen. Results were normalized to ubiquitin, and P values were calculated with Student's t-test.

Primary antibodies:

krt 6 sc-22481; **krt 14** Neomarkes LL002; **krt 10** Covance PRB-159; **Ki67** BD 550609; **E-cad** BD610181 or CS 3195; **Paxillin** BD 610620; **Vinculin** Sigma V9131; **P-MLC2(Ser19)** CS 3675; **MLC2** CS 3672; **aPKCζ** sc-216; **ZO1** Invitrogen 617300; **Par3** Upstate (Millipore) 07–330; **RhoA** CS 2117; **pRB** Pharmigen 554136; **α-tubulin** Sigma T7816; **β-tubulin** AB15246; **Par6** Sigma 9547; and **BrdU** BD 3475800.

Primers:

All 5' to 3'. ***mypt1***: F-gttccagtgaggaggacgag, R-aagccatgggctttgtctta; ***par-6***: F-gggttccaggtatcttcatc, R-gacctcaaggatctcatcac; ***prickle-:*** F-cagagaagctccacatcag R-ggcaagcatgcgaaatag; ***frizzled-2***: F-cacggtcaccacctattt, R-tgcagccttctttcttagt; ***mlc2***: F-gtgttcgccatgtttgac, R-ggcatcagtgggattctt; ***par-3***: F-aacaactgtcccaacgcgagaa, R: tttggttgaggcgtgagcacta; ***ZO1***: F-aaatgagaagcagacgcccact, R-accagtttcatgctgggcctaa; ***aPKCζ***: F-acggacaaccctgacatgaaca, R-tgctgcggaagaaagcatgaga; ***cdc42***: F-tgttggtgatggtgctgttggt, R-agtccaagagtgtatggctctcca; ***rac1***: F-tgcctgctcatcagttacacga, R-ttcttgtccagctgtgtcccat; ***E-cadherin***: F-cagccttcttttcggaagact, R-ggtagacagctccctatgact; ***rock1***: F-gctgaatgacatgcaagcgcaa, R-tttgcccgcaactgctcaat; ***rhoA***: F-tgttggtgatggagcttgtggt, R-tcaaacaccgtgggcacataga; ***p107***: F-tctgacaatggccacaaccaca, R-ttggcgataccatgcaaaggga; ***cyclin E1***: F-tgtttttgcaagacccagatga, R-ggctgactgctatcctcgct.

Results

Rb inactivation causes tissue closure defects during development.

We previously generated *Rb*$^{-/-}$ ES cells constitutively expressing a LacZ reporter to investigate *Rb* mutant tumor phenotypes in chimeric mutant mice [14]. This current study stemmed from our discovery that these *Rb*$^{-/-}$ chimeras displayed tissue closure defects. Specifically, examination at E18.5 revealed partial or complete failure in eyelid closure [called the eyes open phenotype (EOP)] in 39% (15/38) of *Rb*$^{-/-}$ chimeric embryos, as well as sporadic abnormal fusion of the ventral body wall (Fig. 1A). To determine whether these were a direct effect of *Rb* loss, we stained multiple chimeric litters for the LacZ marker of

the $Rb^{-/-}$ cells. Twelve of the 21 embryos examined displayed EOP and/or ventral suture defects and, in every case, LacZ positive ($Rb^{-/-}$) cells comprised the affected site (Fig. 1A). Conversely, embryos with few or no LacZ positive cells at the relevant sites lacked these defects.

Eyelid closure initiates around day E15.5 with formation of the eyelid tip, an epithelial structure that protrudes from each eyelid bud, subsequently extends and migrates over the cornea to fuse in the middle by E16.5 and completely cover the eyes until two weeks post-birth [20]. To evaluate this process in $Rb^{-/-}$ chimeras, we isolated embryos at E16.5 (corresponding to E15.5 in non-chimeras) and conducted immunohistochemical (IHC) staining for keratin 6 (k6), an eyelid tip marker [21]. For 9/9 eyelids with strong LacZ staining at the tip area, this structure had not developed (Fig 1B), while embryos with normal eyelid tips (7/7) had few or no LacZ-positive cells in this region (Fig 1B, Supplemental Fig. 1). Defective *Rb-/-* eyelid tips were characterized by aberrant filamentous (F) actin staining (Supplemental Fig. 1) and frequently accompanied by detachment of the eyelid from the cornea (Fig. 1A-C), both common consequences of mutation of migration genes [20,21]. At later developmental stages, defective eyelid closure was characterized by loss of the leading edge [4/4 *Rb* mutants at E17.5 (Fig. 1B) and 15/15 at E18.5 (Fig. 1A)].

Prior studies have shown that inhibition of cell proliferation does not impair eyelid closure [22] arguing that these processes are unconnected. Nevertheless, constitutive *Rb* inactivation in the basal epidermal layer ($K14CreRb^{c/c}$ mice) yields adult skin with expanded suprabasal layers, which has been reported to result from a combination of ectopic proliferation and differentiation defects [23]. Thus, we examined the eyelid epidermis of E16.5 $Rb^{-/-}$ chimeras for differentiation and proliferation markers. IHC for keratin 14 and 10 revealed no overt differences in either the basal (undifferentiated, k14 positive) or suprabasal (differentiated, k10 positive) epidermal layers of chimeric eyelids with (n=8) or without (n=9) defective tips (Fig 1C, Supplemental Fig. 1). Moreover, in both cases (n=9 each), the area around the eyelid was largely devoid of cells expressing the proliferation marker Ki67 (n≤2 cells; Fig. 1C). Finally, comparison of E18.5 chimeras generated with $Rb^{-/-}$ versus $Rb^{-/-};E2f3^{-/-}$ or $Rb^{-/-};E2f4^{-/-}$ ES cells showed that the EOP of *Rb* mutants was unaltered by the simultaneous loss of *E2f3* or *E2f4* (Supplemental Fig. 1). Thus, *Rb* loss causes tissue closure defects that arise independent of either differentiation or proliferation defects, or from deregulation of *E2f* transcription factors that account for many other embryonic *Rb* mutant phenotypes.

To further explore the breadth of pRB's role in tissues closure, we also analyzed the effect of *Rb* deficiency on wound healing. For this, we generated $K14CreER^{+};Rb^{c/c}$ mice in which tamoxifen treatment allows *Rb* deletion in the basal epidermal layer. To highlight the contribution of migration during wound closure, we used skin-thick incisions, rather than patch-excision, to minimize the impact of ectopic proliferation caused by *Rb* loss in the epidermis [23]. We painted the skin of adult $Rb^{c/c}$ (wildtype) or $K14CreER^{+};Rb^{c/c}$ (*Rb* mutant) mice with tamoxifen daily for 11 days (which is sufficient for *Rb* deletion, Supplemental Fig. 1), then performed a 1 cm cut and monitored wound healing. After 5 days, healing was completed in wildtype but not mutant skins (Fig. 1D), indicating that *Rb* deficiency impairs wound healing, despite efficient expression of keratin 6 (Fig. 1D), which is essential for this process. This likely reflects a delay, not complete abrogation, of the

healing response since healing was evident at the extremes of the wound in *Rb* mutant skin (Fig 1D). Thus, *Rb* is required for appropriate tissue closure in normal development and adult tissue homeostasis.

pRB regulates cell motility.

The closure defects we observed in *Rb* mutants are reminiscent of defects resulting from motility gene mutations [20,21], suggesting that *Rb* somehow regulates migration. To address this, we examined the effect of *Rb* loss on primary epithelial cells. We isolated keratinocytes from the skin of E18.5 $Rb^{c/c}$ embryos and infected them with adenoviruses expressing GFP alone or Cre-GFP, to create matched wildtype and $Rb^{-/-}$ cells. All subsequent analyses were conducted 48 hours post-infection, when pRB was undetectable in the Cre-infected cells (Supplemental Fig. 2). Initially, we cultured confluent keratinocyte monolayers in high calcium for at least 24 hours to induce cell-cell junctions, differentiation, and formation of *in vitro* "skins", which we then scratched and monitored for healing capacity. By the time the wildtype cells had completely filled the scratch (30 hours), the *Rb* mutant cells had covered only 60% of the wounded area (Fig. 2A). Notably, as previously reported [23], analysis of BrdU incorporation showed that the wildtype cells were completely arrested while the *Rb* mutants were undergoing ectopic proliferation (Fig. 2A). Interestingly, increased cell proliferation generally correlates with increased healing ability [24]. In stark contrast, our data show that *Rb* mutation causes healing defects even in the presence of increased proliferation.

We also wished to separate cell migration defects from cell proliferation defects. For this, we employed low calcium conditions in which wildtype and *Rb* mutant cells display comparable proliferation rates (Fig. 2B), as previously reported [23]. Since low calcium does not allow formation of cell junctions and thus epithelial cell layers, we assessed migration of single cells using modified Boyden chambers. After 12 hours, only 30% of $Rb^{-/-}$ cells had migrated to the chamber bottom compared to wildtype controls (Fig. 2B). Thus, pRB is required for appropriate cell migration independent of its role in cell division. To further define the nature of the migratory defects, we performed time-lapse microscopy on cultured single cells over a 15 hour period. Analysis of the cell tracks showed that $Rb^{-/-}$ keratinocytes covered 25% less distance and were 65% slower than the wildtype controls (Fig. 2C). Moreover, the $Rb^{-/-}$ keratinocytes had a 50% reduced persistence (the ability to maintain a specific trajectory; Fig. 2C), which suggested a problem with cell polarity.

Rb modulates Rho activity in epithelial cells.

In addition to their migratory defects, the $Rb^{-/-}$ keratinocytes were rounder than their wildtype controls, showing a 25% increase in circularity index (Fig. 3A, Supplemental Fig. 3). This indicates an impaired ability to establish front-back polarity, which is indispensable for productive migration and is dictated by RhoGTPase activity. Examination of the time lapse images indicated that the $Rb^{-/-}$ cells could still form protrusions (not shown). However, these cells possessed prominent stress fibers [detected by staining for filamentous actin (phalloidin)] that were arranged across the cell body, in stark contrast to wildtypes, in which stress fibers were restricted to the periphery and more to one side (Fig. 3A). These phenotypes, suggesting that *Rb* loss causes a shift towards a less polarized state, were

coupled with a significant increase ($p<0.0001$) in the mean area of focal adhesions (FA; from 569±23 pixels for wildtype controls to 1118±43 pixels for *Rb-/-* cells), as determined by immunofluorescence (IF) staining for vinculin (Fig. 3A) and paxillin (Fig. 3C), indicating stronger substrate attachment. Increased stress fibers and thicker FAs are consistent with impaired cell motility and are generally caused by hyperactive RhoA [2]. RhoA stimulates Rock kinase activity and thus myosin light chain 2 (MLC2) phosphorylation, thereby regulating cell contractility. We found that *Rb* loss caused no appreciable change in the mRNA levels for RhoA (or the prototypical Rho GTPases, Rac and Cdc42) or the total protein levels of RhoA and its effectors (Supplemental Fig. 3, data not shown). However, it clearly increased the levels of phosphorylated myosin light chain 2 (P-MLC2, Fig. 3B) and the inhibitory phosphorylation of the MLC2 phosphatase (P-Thr853-MYPT1), another known Rock substrate (Supplemental Fig. 3). Rac and Cdc42 can also modulate MLC2 phosphorylation, acting via Rock independent mechanisms [1]. Thus, to assess whether these defects result from RhoA hyperactivation, we tested the effect of two distinct Rock inhibitors, H1152 and Y27632. Treatment for 1 hour significantly reduced the levels of P-MLC2 in both wildtype and $Rb^{-/-}$ cells (Fig. 3B), and yielded a concomitant decrease in stress fibers and FA (Fig. 3C). Together, these data establish a role for *Rb* in the regulation of stress fibers and FA through activation of the RhoA-Rock axis at the post-transcriptional level.

Rb controls cell and tissue architecture.

The existence of a pRB-RhoA pathway link, together with the effects of *Rb* loss on cell morphology and motility, suggest a regulatory role for pRB in general tissue polarity. Notably, the skin of $K14CreRb^{c/c}$ mice, which have constitutive *Rb* deletion in the basal layer, has abnormal architecture, extra cell layers, sparse hair and enlarged sebaceous glands [23] (Fig. 4A). These phenotypes, have been previously ascribed to ectopic proliferation and improper differentiation [23] but we hypothesized that they might reflect intrinsic defects in asymmetric cell division and/or altered self-renewal, which both involve cell polarity. Consistent with this notion, we found that $K14CreRb^{c/c}$ mice have rough coats (Fig. 4A) suggesting a defect in hair orientation. Notably, appropriate hair orientation requires establishment of planar cell polarity (PCP) in the basal layer of the interfollicular epidermis, which occurs prior to stratification and independent of proliferation [25]. Importantly, the mechanisms underlying PCP share commonalities with those used to close epithelial wounds and regulate directional migration. To probe the effect of *Rb* loss on tissue architecture, we analyzed the adult skin of $K14CreRb^{c/c}$ ($Rb^{-/-}$) mice, versus *K14Cre* (wildtype) littermates, for F-actin (phalloidin staining) and polarity determinants. Phalloidin and DAPI staining showed that the $Rb^{-/-}$ cells were both misshapen and bigger than wildtypes, and their nuclei were misoriented (Fig. 4B). Moreover, two key components of the PAR complex, aPKCζ and Par3, had disrupted localization at both the cell and tissue levels. Within cells, these proteins were diffusely distributed at the cell membrane in *Rb* mutants and also in the cytoplasm in the case of Par3, in contrast to discrete membrane localization in wildtypes (Fig. 4B). At the whole tissue level, aPKCζ expression was mostly restricted to the basal layer and Par3 to the suprabasal layers in wildtypes, but both proteins were present in both layers of the $Rb^{-/-}$ epidermis (Fig 4B). Despite their differential PAR protein localization, wildtype and $Rb^{-/-}$ epidermal cells displayed similar membranous localization of the

adherens and tight junction markers, E-cadherin and ZO1 (data not shown), consistent with the reported intact skin barrier in *Rb* deficient skin [23]. Thus, *Rb* loss alters the distribution of a subset of proteins that define polarity in adult skin, and causes skin architecture defects characteristic of polarity/PCP defects.

Our *in vivo* analyses do not rule out the possibility that altered PAR protein distribution is a secondary effect of ectopic proliferation and/or extra cell layers within *Rb* mutant skin, as opposed to a distinct consequence of *Rb* depletion. To address this, we used our *in vitro* system to mimic the formation of an epithelium, including establishment of apical basal polarity and junction formation, by stimulating subconfluent monolayers of wildtype and $Rb^{-/-}$ keratinocytes with calcium for 3 to 24 hrs. In wildtype primary keratinocytes, 3 hrs calcium treatment is known to induce cytoskeleton remodeling in adjacent cells with formation of circular belts and F-actin-rich intercalating finger-like protrusions called punctae that contain immature junctions [26]. With continued calcium exposure, the polarity proteins allow the vertical stratification of tight (TJ) and adherens junctions (AJ), with TJs more apical, and F-actin and myosin remodeling with formation of apical junctional belts. By 24 hrs the apical basal program is complete and the junctions are fully “mature”. In our analyses, at the 3 hrs timepoint, adjacent wildtype cells had appropriately remodeled their actin-myosin cytoskeleton to generate defined circular belts, but F-actin and myosin were disorganized and diffused, with aberrant rings at the cell-cell junctions, in $Rb^{-/-}$ cells (Fig. 4C). This *Rb* mutant phenotype was accompanied by a significant upregulation of the polarity proteins, Par6 (data not shown), Par3 and aPKC (Fig. 4C), at the cell membrane. Moreover, while E-cadherin (AJ) and ZO1 (TJ) localized appropriately at punctae in adjacent wildtype cells, $Rb^{-/-}$ keratinocytes had significantly fewer projections and an increased frequency of flat and continuous E-cadherin and ZO1 positive areas (Fig. 4D). Importantly, these effects were clearly independent of pRB’s role in proliferation and differentiation, as wildtype and $Rb^{-/-}$ cells proliferate at comparable rates after 3 hrs of calcium treatment (Supplemental Fig. 4). This spectrum of $Rb^{-/-}$ defects occurred without any detectable increase in the levels of RNA or protein (either total or active phosphorylated species) for these deregulated polarity and junction proteins (Supplemental Fig.4). 24 hours post-calcium, wildtype cells achieved full junctional maturity, as expected, but defects in actin cytoskeleton, PAR proteins accumulation, and aberrant junctional complexes remained evident in $Rb^{-/-}$ epithelial layers (Fig 4E, Supplemental Fig.4) indicating that these are not transitory and could explain, or contribute to, the altered structure in the mutant adult skin. Interestingly, our data suggest that the effects of *Rb* loss on tissue polarity are, at least in part, Rho independent. Specifically, we cultured the epithelial layers with Rock inhibitors for the final hour of the 3 hour calcium treatment but this did not reverse the aberrant accumulation of aPKC at the cell membranes of $Rb^{-/-}$ cells despite disrupting the acto-myosin cytoskeleton in both wildtype and mutant cells (Supplemental Fig.4, not shown). Thus, collectively our data show that *Rb* inactivation impairs establishment of polarity in a forming epithelium by interfering with the basic polarity machinery independently of proliferation.

p53 mutation selectively rescues motility in Rb-deficient cells.

Tumor progression features loss of polarity and deregulated migration and invasion. Our data show that *Rb* inactivation causes loss of polarity, while simultaneously reducing migration, thereby yielding apparently conflicting effects. This was unexpected given the significant link between *RB* inactivating mutations and highly metastatic human tumors such as retinoblastoma, osteosarcoma, and small cell lung cancer. We therefore hypothesized that additional mutations are needed to overcome the hypomotile state imposed by *Rb* loss. We noted that *Tp53* is frequently mutated in *RB-1* mutant tumors. Moreover, *Rb* deletion is not sufficient to initiate skin cancer, while concomitant inactivation of *tp53* allows early onset, metastatic squamous cell carcinomas [27]. Thus, we tested whether *tp53* loss could modulate the *Rb*-deficient epithelial phenotypes by generating *K14*Cre$Rb^{c/c};p53^{c/c}$ and *K14*Cre$p53^{c/c}$ mice. As reported [27], mutation of *tp53* alone did not alter skin composition or morphology (data not shown). When combined with *Rb* loss, the resulting *Rb;p53* DKO skins showed a similar, altered architecture to *Rb* single mutants, including thicker, disorganized epidermis, enlarged sebaceous glands and misoriented hair (Fig. 5A), suggesting that *tp53* loss does not modulate the altered polarity of the $Rb^{-/-}$ cells. To directly test this, we generated paired *Rb;p53* DKO and wildtype keratinocytes, by infecting $Rb^{c/c};p53^{c/c}$ keratinocytes with Ad-CreGFP or Ad-GFP. In response to 3 hour calcium, the *Rb;p53* DKO cells showed the same upregulation of aPKC at junctional membranes and altered cytoskeleton, as the $Rb^{-/-}$ cells (compare Fig. 5B to Fig 4C), confirming retention of their polarity defects. We then used *in vitro* scratch assays to assess cell motility. Remarkably, the *Rb;p53* DKO cells healed the *in vitro* wound at the same rate as their wildtype controls (Fig. 5C). Thus, *p53* mutation overrides the hypomotility of $Rb^{-/-}$ cells (Fig. 5C). To characterize this further, we then analyzed these cells in low calcium and low confluence. The *Rb;p53* DKOs maintained the higher circularity index of $Rb^{-/-}$ keratinocytes (compare Fig. 5D to Fig. 3A) but simultaneously displayed a dramatic difference in the FA phenotype; while FAs of $Rb^{-/-}$ cells were almost double the size of their wildtype counterparts (Fig. 3A), the mean FA size was significantly smaller ($p<0.0001$) for *Rb;p53* DKO cells than their wildtype controls (Fig. 5D; 568±23 pixels for DKO versus 759±23 pixels for wildtypes). Accompanying this FA change, the levels of the RhoA effector, P-MLC2, were the same in *Rb;p53* DKO and wildtype cells, and not elevated as in *Rb* single mutants (Fig. 5D). Thus, *tp53* mutation does not “correct” the polarity defect resulting from *Rb* loss, but it fully rescues the hypomotility, possibly by modulating focal adhesions, and restoring Rho activity to normal.

Discussion

Our work highlights an unappreciated role for pRB in epithelial cell migration and polarity that is independent of cell proliferation. The extensive crosstalk between these two processes is well established, and undoubtedly occurs in our *Rb* deficient cells. However, our data show that *Rb* loss derails these processes through separable mechanisms, as evidenced by the differential rescue occurring upon *tp53* loss. Our data indicate that the migration defects reflect deregulation of RhoA activity. The precise mechanism by which pRB loss achieves this is unclear, but it is not mediated at the level of RhoA transcription. Consistent with the notion of *Rb*-RhoA cross-talk, deregulation of RhoA or Rock yields phenotypes similar to

the ones described above for *Rb* loss. RhoA hyperactivation decreases, and knockdown increases, collective epithelial cell migration in scratch assays [28]. Rock overexpression causes epidermal thickening [29], and its inactivation leads to decreased stress fibers in primary keratinocytes and tissue closure defects [21]. While our study is the first to describe pRB-RhoA crosstalk in primary epithelial cells, interactions between *Rb* and RhoGTPases seem relevant in other cell contexts. *Rb* loss upregulates Rac activity in osteoblasts [30], and mimics the effects of RhoA activation in prostate cancer cells by promoting actin polymerization through E2F-dependent upregulation of RHAMM [12]. Interestingly, in both prostate and breast cancer cells, *Rb* deficiency also augments metastases by decreasing cell-cell adhesion and induction of EMT [12,31], but these mechanisms do not seem to be engaged in our *Rb* deficient keratinocytes (Supplemental Fig. 4).

Our study also showed that pRB is necessary for the establishment of polarity during formation of an epithelial layer. The aberrant polarity resulting from *Rb* loss occurs independent of ectopic proliferation, at least *in vitro*, and is sufficient to disrupt the localization of PAR complex components and the establishment of apical-basal polarity during epithelial layer formation. Notably, the defects in PAR complex component localization are also apparent in *Rb* mutant skin, suggesting that the aberrant skin architecture reflects alterations in tissue polarity, asymmetric cell division and PCP. While our study is the first to establish pRB's role in apical-basal polarity in epithelial cells, we note that pRB was recently implicated in PCP in the Drosophila wing and eye [13]. In this invertebrate context, the effect of *Rb* loss on PCP was linked to modest transcriptional changes in *pk*, *vang*, *fmi* and, of relevance to our study, *aPKC*. However restoration of *aPKC* levels did not impact the *Rb* mutant wing defects and only partially rescued the eye [13]. The expression of these genes is not altered in our *Rb* deficient keratinocytes (Supplemental Fig. 4), but these findings suggest that *Rb*'s role in polarity is evolutionarily conserved.

Our study also has intriguing implications for the tumorigenic consequences of *Rb* inactivation. At a simplistic level, deregulated polarity would appear to be tumor promoting, while hypomotility might seem tumor suppressive, although this could be context dependent. In the colon for instance, where epithelial cells move quickly from the bottom to the top of the crypts before shedding, decreased migration might increase the cells' lifetime and thus facilitate tumor development. This mechanism, recently suggested for *Apc* [32], would fit our prior finding that *Rb* inactivation promotes colorectal cancer [33]. In other tissues, reduced migration could be anti-tumorigenic. One such case, could be two-step skin carcinogenesis, were *Rb* mutant skin yields fewer tumors than *Rb* wildtype. Interestingly, over time, these *Rb* deficient tumors actually become more invasive than their *Rb* wildtype counterparts [34]. Given our findings, we speculate that the *Rb* deficient epithelial cells are "pre-primed" to be tumorigenic because of the loss of polarity but initially disabled by their hypomotility, and that the subsequent acquisition of additional mutations – in our case specifically the loss of *tp53* – releases this migratory block and unleashes invasiveness. This model fits with the increased onset, incidence and aggressiveness of squamous cell carcinomas observed in *Rb;p53* versus *p53* murine deficient skin, and explains the prevalence of *RB-1* and *Tp53* co-mutation in highly metastatic human tumor types, such as retinoblastoma, osteosarcoma and SCLC. While a systematic analysis of migration and polarity regulators in *Rb* deficient tumors remains to be done, this work suggests that

inhibitors or agonists of polarity factors and RhoA/Rock might be an interesting option for treatment of *RB-1* mutant metastatic tumors.

Supplementary Material

Refer to Web version on PubMed Central for supplementary material.

Acknowledgements

We thank Roberta Ferretti, Scott R. Frank and Craig Furman for reagents and ideas, and the Koch Institute Swanson Biotechnology Center for technical support, especially the Microscopy and Histology Cores. Funding for this study was provided by PO1-CA42063 from NIH/NCI and also supported in part by the Koch Institute Support (core) Grant P30-CA14051 from NIH/NCI. J.A.L. is the Virginia and D.K. Ludwig Professor for Cancer Research at the Koch Institute for Integrative Cancer Research.

References

1. Guilluy C, Garcia-Mata R, Burridge K. Rho protein crosstalk: another social network? Trends Cell Biol 2011;21(12):718–726. [PubMed: 21924908]
2. Ridley AJ. Rho family proteins: coordinating cell responses. Trends Cell Biol 2001;11(12):471–477. [PubMed: 11719051]
3. Etienne-Manneville S, Hall A. Cell polarity: Par6, aPKC and cytoskeletal crosstalk. Curr Opin Cell Biol 2003;15(1):67–72. [PubMed: 12517706]
4. Goldstein B, Macara IG. The PAR proteins: fundamental players in animal cell polarization. Dev Cell 2007;13(5):609–622. [PubMed: 17981131]
5. Vega FM, Ridley AJ. Rho GTPases in cancer cell biology. FEBS Lett 2008;582(14):2093–2101. [PubMed: 18460342]
6. Iden S, Collard JG. Crosstalk between small GTPases and polarity proteins in cell polarization. Nat Rev Mol Cell Biol 2008;9(11):846–859. [PubMed: 18946474]
7. Zallen JA. Planar polarity and tissue morphogenesis. Cell 2007;129(6):1051–1063. [PubMed: 17574020]
8. Martin-Belmonte F, Perez-Moreno M. Epithelial cell polarity, stem cells and cancer. Nat Rev Cancer 2012;12(1):23–38.
9. Waclaw B, Bozic I, Pittman ME, Hruban RH, Vogelstein B, Nowak MA. A spatial model predicts that dispersal and cell turnover limit intratumour heterogeneity. Nature 2015;525(7568):261–264. [PubMed: 26308893]
10. Dyson NJ. RB1: a prototype tumor suppressor and an enigma. Genes Dev 2016;30(13):1492–1502. [PubMed: 27401552]
11. Ferguson KL, McClellan KA, Vanderluit JL et al. A cell-autonomous requirement for the cell cycle regulatory protein, Rb, in neuronal migration. EMBO J 2005;24(24):4381–4391. [PubMed: 16308563]
12. Thangavel C, Boopathi E, Liu Y et al. RB Loss Promotes Prostate Cancer Metastasis. Cancer Res 2016;77(4):982–995. [PubMed: 27923835]
13. Payankaulam S, Yeung K, McNeill H, Henry RW, Arnosti DN. Regulation of cell polarity determinants by the Retinoblastoma tumor suppressor protein. Sci Rep 2016;6:22879. [PubMed: 26971715]
14. Parisi T, Yuan TL, Faust AM, Caron AM, Bronson R, Lees JA. Selective requirements for E2f3 in the development and tumorigenicity of Rb-deficient chimeric tissues. Mol Cell Biol 2007;27(6): 2283–2293. [PubMed: 17210634]
15. Parisi T, Bronson RT, Lees JA. Inhibition of pituitary tumors in Rb mutant chimeras through E2f4 loss reveals a key suppressive role for the pRB/E2F pathway in urothelium and ganglionic carcinogenesis. Oncogene 2009;28(4):500–508. [PubMed: 18997819]

16. Sage J, Mulligan GJ, Attardi LD et al. Targeted disruption of the three Rb-related genes leads to loss of G1 control and immortalization. Genes Dev 2000; 14(23):3037–3050. [PubMed: 11114892]
17. Dassule HR, Lewis P, Bei M, Maas R, McMahon AP. Sonic hedgehog regulates growth and morphogenesis of the tooth. Development 2000;127(22):4775–4785. [PubMed: 11044393]
18. Vasioukhin V, Degenstein L, Wise B, Fuchs E. The magical touch: genome targeting in epidermal stem cells induced by tamoxifen application to mouse skin. Proc Natl Acad Sci U S A 1999;96(15):8551–8556. [PubMed: 10411913]
19. Hodivala-Dilke KM, DiPersio CM, Kreidberg JA, Hynes RO. Novel roles for alpha3beta1 integrin as a regulator of cytoskeletal assembly and as a trans-dominant inhibitor of integrin receptor function in mouse keratinocytes. J Cell Biol 1998;142(5):1357–1369. [PubMed: 9732295]
20. Xia Y, Kao WW. The signaling pathways in tissue morphogenesis: a lesson from mice with eye-open at birth phenotype. Biochem Pharmacol 2004;68(6):997–1001. [PubMed: 15313393]
21. Shimizu Y, Thumkeo D, Keel J et al. ROCK-I regulates closure of the eyelids and ventral body wall by inducing assembly of actomyosin bundles. J Cell Biol 2005;168(6):941–953. [PubMed: 15753128]
22. Heller E, Kumar KV, Grill SW, Fuchs E. Forces generated by cell intercalation tow epidermal sheets in mammalian tissue morphogenesis. Dev Cell 2014;28(6):617–632. [PubMed: 24697897]
23. Ruiz S, Santos M, Segrelles C et al. Unique and overlapping functions of pRb and p107 in the control of proliferation and differentiation in epidermis. Development 2004;131(11):2737–2748. [PubMed: 15148303]
24. Schafer M, Werner S. Cancer as an overhealing wound: an old hypothesis revisited. Nat Rev Mol Cell Biol 2008;9(8):628–638. [PubMed: 18628784]
25. Devenport D, Fuchs E. Planar polarization in embryonic epidermis orchestrates global asymmetric morphogenesis of hair follicles. Nat Cell Biol 2008;10(11):1257–1268. [PubMed: 18849982]
26. Vasioukhin V, Bauer C, Yin M, Fuchs E. Directed actin polymerization is the driving force for epithelial cell-cell adhesion. Cell 2000;100(2):209–219. [PubMed: 10660044]
27. Martinez-Cruz AB, Santos M, Lara MF et al. Spontaneous squamous cell carcinoma induced by the somatic inactivation of retinoblastoma and Trp53 tumor suppressors. Cancer Res 2008;68(3): 683–692. [PubMed: 18245467]
28. Zaritsky A, Tseng YY, Rabadan MA et al. Diverse roles of guanine nucleotide exchange factors in regulating collective cell migration. J Cell Biol 2017;216(6):1543–1556. [PubMed: 28512143]
29. Samuel MS, Lopez JI, McGhee EJ et al. Actomyosin-mediated cellular tension drives increased tissue stiffness and beta-catenin activation to induce epidermal hyperplasia and tumor growth. Cancer Cell 2011;19(6):776–791. [PubMed: 21665151]
30. Sosa-Garcia B, Gunduz V, Vazquez-Rivera V et al. A role for the retinoblastoma protein as a regulator of mouse osteoblast cell adhesion: implications for osteogenesis and osteosarcoma formation. PLoS One 2010;5(11):e13954. [PubMed: 21085651]
31. Arima Y, Inoue Y, Shibata T et al. Rb depletion results in deregulation of E-cadherin and induction of cellular phenotypic changes that are characteristic of the epithelial-to-mesenchymal transition. Cancer Res 2008;68(13):5104–5112. [PubMed: 18593909]
32. Juanes MA, Bouguenina H, Eskin JA, Jaiswal R, Badache A, Goode BL. Adenomatous polyposis coli nucleates actin assembly to drive cell migration and microtubule-induced focal adhesion turnover. J Cell Biol 2017;216(9):2859–2875. [PubMed: 28663347]
33. Parisi T, Bronson RT, Lees JA. Inactivation of the retinoblastoma gene yields a mouse model of malignant colorectal cancer. Oncogene 2015;34(48):5890–5899. [PubMed: 25745996]
34. Ruiz S, Santos M, Lara MF, Segrelles C, Ballestin C, Paramio JM. Unexpected roles for pRb in mouse skin carcinogenesis. Cancer Res 2005;65(21):9678–9686. [PubMed: 16266987]

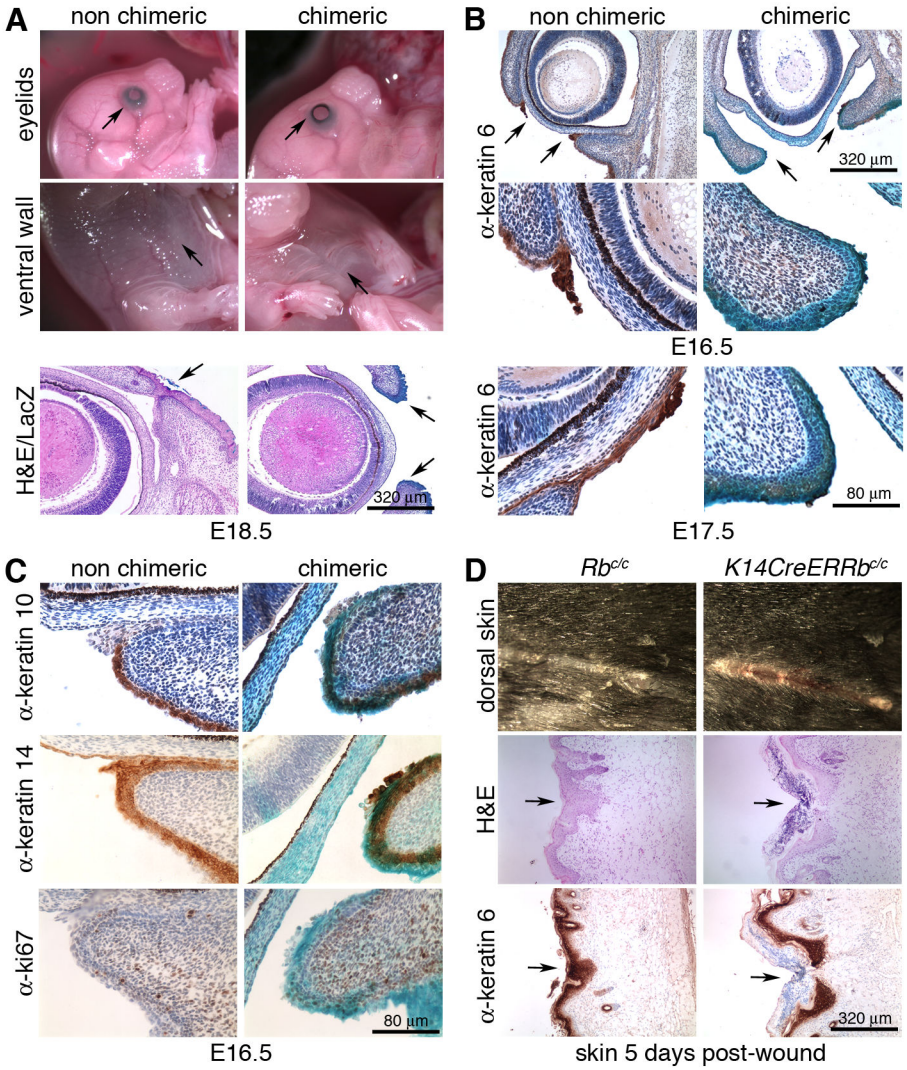

Figure 1. *Rb* inactivation causes general tissue fusion defects.

(A) Representative images of E18.5 *Rb* null chimeric embryos displaying EOP and aberrant body wall fusion (upper panel). H&E counterstaining of whole mount LacZ stained sections showed co-occurrence of the EOP defect and $Rb^{-/-}$ (blue) cells at the eyelid end (lower panel). (B) Representative images of IHC of E16.5 (upper panel) and E17.5 (lower panel) embryos with α-k6 showed failure to form the tip in $Rb^{-/-}$ eyelids. (C) IHC for k10, k14 and Ki67 at E16.5 showed that the differentiated and basal layers are equally represented in $Rb^{-/-}$ chimeric mutant and non-chimeric eyelid epidermis, and that proliferation is negligible in both. (D) Representative images five days after wounding, showed a delay in wound closure in *Rb*-deficient skin, relative to the wildtype control (upper panel), despite displaying efficient k6 expression (lower panel).

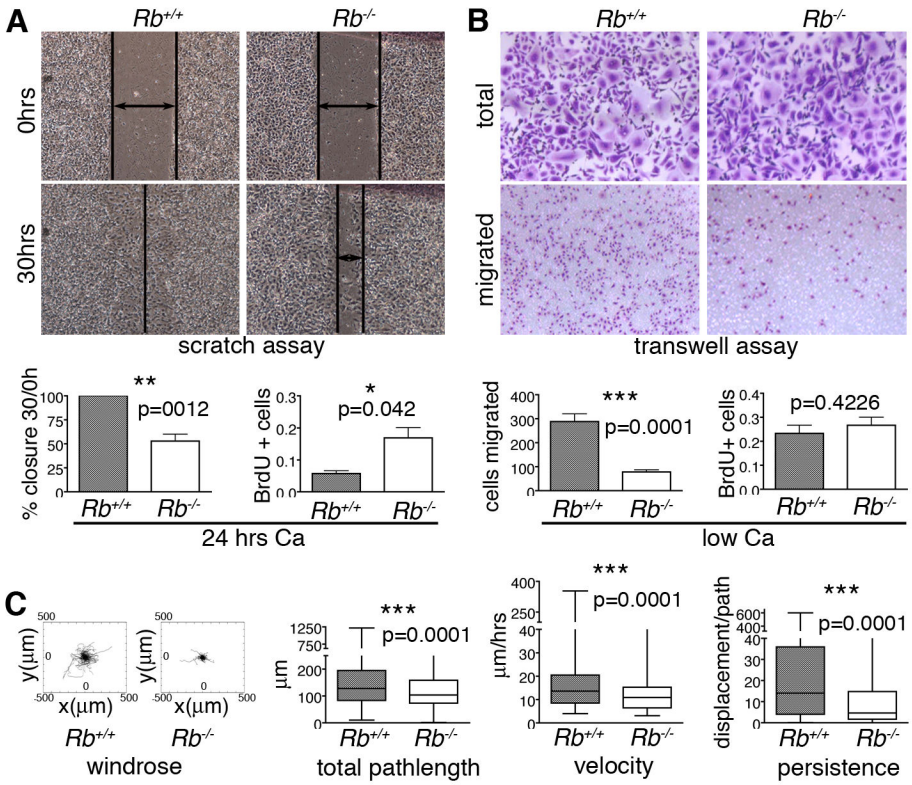

Figure 2. *Rb* null keratinocytes have motility defects.

(A) Epithelial cell layers were generated by culturing wildtype and $Rb^{-/-}$ keratinocytes in high calcium for 24 hours. The $Rb^{-/-}$ keratinocytes had an impaired ability to repair scratches, as indicated by representative images and quantification (left graph; n=6 lines), and displayed ectopic proliferation, as assessed by BrdU incorporation (right graph; 3 lines/genotype, ~2000 cells. (B) Single $Rb^{-/-}$ keratinocytes (cultured in low calcium) showed impaired migration 12 hrs post-plating in Boyden chambers relative to wildtype controls, as judged by crystal violet staining of cells with representative images above and quantification in left graph (n=6 lines/genotype, plated in triplicate), without proliferation changes, which were assessed by BrdU incorporation (right graph; n=3 lines/genotype, ~500 cells). (C) Time-lapse microscopy was conducted for 15 hrs to track the path of individual wildtype and $Rb^{-/-}$ keratinocytes (n=3 lines and >350 cells per genotype). From left to right: windrose plots and graphs show that $Rb^{-/-}$ cells had significant reduced total pathlength, velocity, and persistence compared to their wildtype counterparts. Statistical significance was determined by Student's t-test.

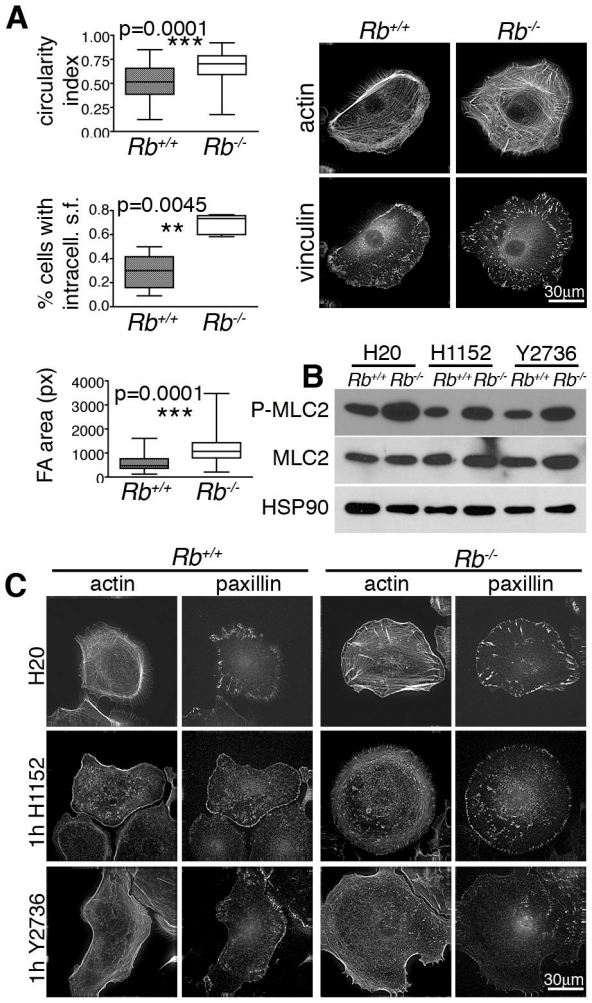

Figure 3. *Rb* loss causes changes in cell architecture that correlate with hyperactive RhoA.

(A) Compared to wildtype controls, single *Rb*$^{-/-}$ keratinocytes had a higher circularity index (n=3 lines/genotype, ~300 cells) indicating reduced polarization, and displayed more prominent non-peripheral stress fibers (phalloidin staining for F-actin; n=5 lines/genotype, >90 cells) and FAs that were larger and more localized within the cell body (α-vinculin IF; n= 3 lines/genotype, >150 cells). Significance was determined by Student's t-test. (B) Wildtype and *Rb*$^{-/-}$ keratinocytes grown as single cells in low calcium with or without 1hr treatment with two different Rock inhibitors, H1152 and Y2673. Western blotting showed that *Rb*-deficiency caused increased levels of P-MLC2, which was reversed by the Rock inhibitors indicating that this is dependent on hyperactive Rho/Rock. (C) 1 hr treatment with H1152 and Y2673 (n= 3 lines/genotype, 80 cells) resulted in loss of the stress fibers (phalloidin staining for actin), including the aberrant fibers across the body of *Rb-/-* cells, and altered FAs (α-paxillin IF) by both reducing their size and eliminating the intracellular localization characteristic of *Rb*$^{-/-}$ cells.

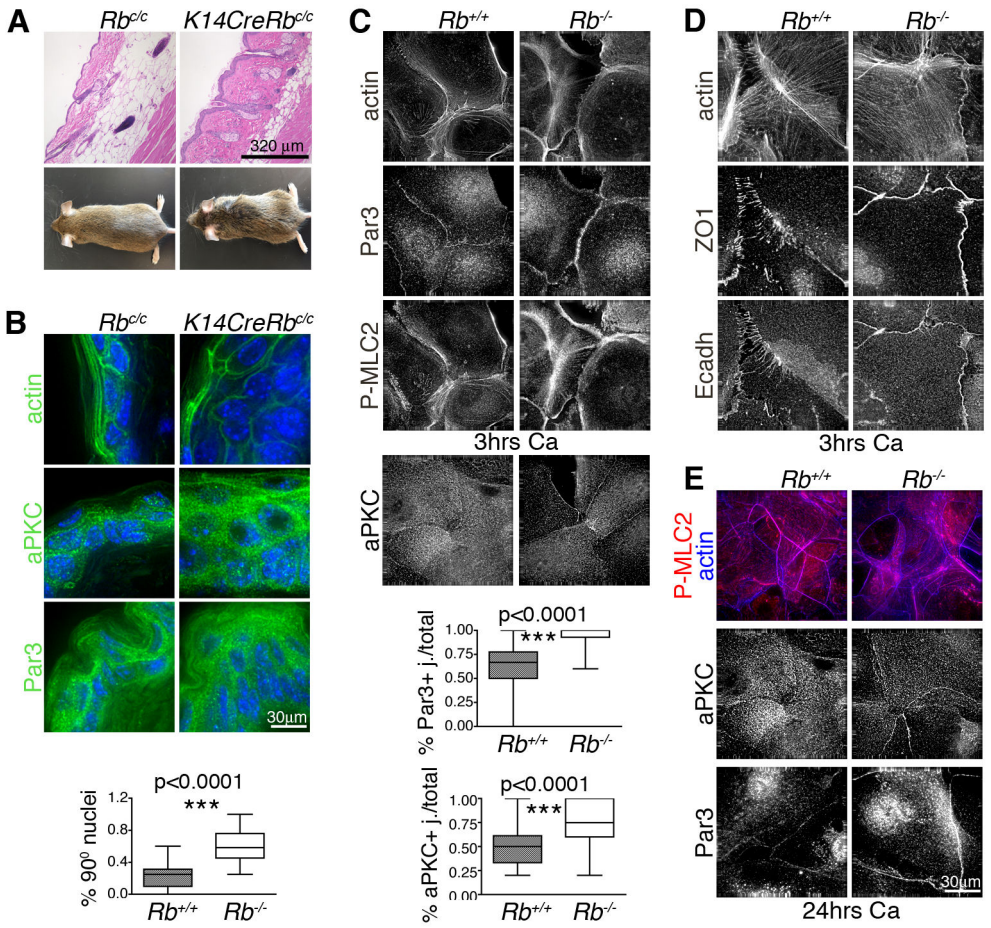

Figure 4. *Rb* inactivation in the epidermis causes polarity defects.

Skin from mice with constitutive *Rb* mutation in the basal layer (n=4) showed: (A) disorganized skin architecture, misoriented hair and enlarged sebaceous glands (H&E sections) and sparse hair and rough coats (mouse pictures); and (B) aberrant tissue morphology (phalloidin staining of actin cytoskeleton) and nuclei orientation (DAPI), with Par3 and aPKC less restricted at the cell membrane and mislocalized within the epidermal layers (IF images). (C, D) Wildtype and $Rb^{-/-}$ keratinocytes were cultured in high calcium for 3 hours to trigger cell junction formation. (C) The $Rb^{-/-}$ keratinocytes (n>6 lines/genotype, ~ 500 cells) showed stress fibers (phalloidin staining) crossing the cells' basal surface and aberrant phospho-myosin (P-MLC2) and actin rings at the cell-cell junctions. Additionally Par3 and aPKC were upregulated at the cell membrane (n>3 lines/genotype. The graphs show the number of Par3 and aPKC positive junctions calculated over the total number of touching cell sides (n=294 and 210 respectively). (D) Adherens junctions (E-cadherin staining) and tight junctions (ZO1 staining) were localized in continuous lines in $Rb^{-/-}$ cells versus punctae in wildtype controls. (E) Wildtype and $Rb^{-/-}$ keratinocytes were maintained in high calcium for 24 hours. The acto-myosin cytoskeletal defects, and Par3 and aPKC upregulation, persisted in $Rb^{-/-}$ keratinocytes at this time. Statistical significance was determined by Student's t-test.

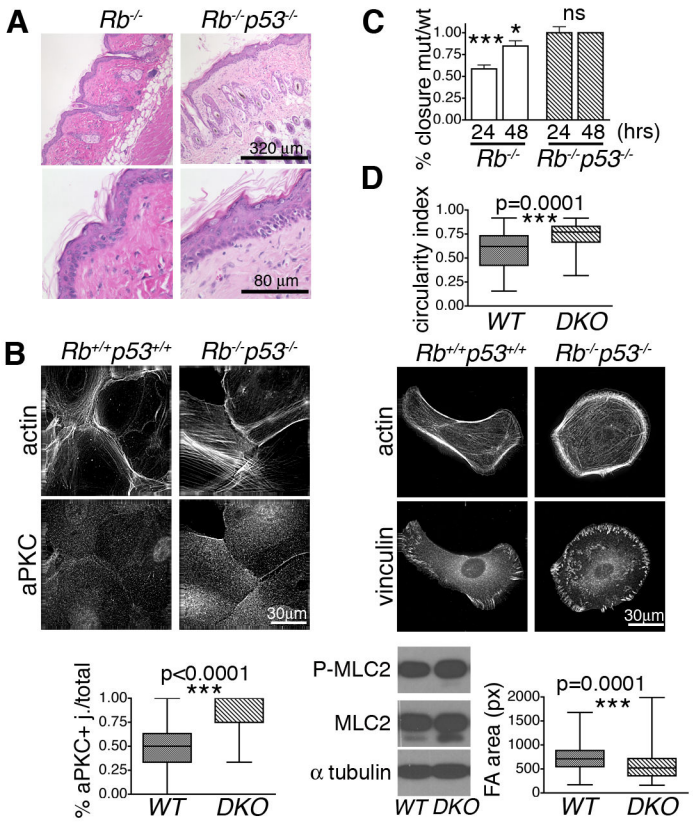

Figure 5. *tp53* inactivation in *Rb* deficient epithelial cells rescues the migration but not the polarity defect.

(A) Representative H&E sections show that *Rb* and *Rb;p53* deficient adult skins were thicker, had misoriented hairs and aberrant sebaceous glands (n=11/genotype). (B) *Rb;p53* DKO keratinocytes, induced with high calcium for 3 hours, showed aPKC upregulation (n=222 cells) in a similar manner to $Rb^{-/-}$ (see Fig. 4C). (C) *Rb;p53* DKO or *Rb-/-* cells were cultured in high calcium for 24 hours alongside their paired wildtype controls, to allow epithelial layer formation, and then subjected to scratch assays (n≥3 lines/genotype). The graphs (comparing healing to wildtype controls at 24 and 48 hours) showed that the *Rb;p53* DKO cells closed the wound in a comparable manner to wildtypes, in contrast to the impaired healing of $Rb^{-/-}$ cells. (D) Wildtype and *Rb;p53* DKO cells were cultured as single cells in low calcium. The graph, showing measurement of the circularity index establishes that the *Rb;p53* DKO cells maintain the front back polarity defect (n=3 lines/genotype, 67 cells) present in the single $Rb^{-/-}$ keratinocytes (see Fig. 3A). In contrast, IF staining showed that the *Rb;p53* DKO cells had smaller FAs (vinculin staining; n=3 lines/genotype, 174 cells) than their wildtype controls, which correlated with wildtype levels of P-MLC2 and total MLC2. Statistical significance was determined by Student's t-test. ***p≤0.0001. *p≤0.01.